# GROUND DATA PROCESSING & PRODUCTION OF THE LEVEL 1 HIGH RESOLUTION MAPS

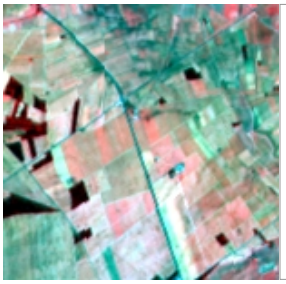

**VALERI 2004**

**Plan-de-Dieu site**
(crops)

**Philippe Rossello**

April 2007

**CONTENTS**

# 1. Introduction

This report describes the production of high resolution, level 1, biophysical variable maps for the Plan-de-Dieu site in 2004 (see campaign report for more details about the site and the ground measurement campaign: annex or http://www.avignon.inra.fr/valeri). Level 1 map corresponds to the map derived from the determination of a transfer function between reflectance values of the SPOT image acquired during (or around) the ground campaign, and biophysical variable measurements (hemispherical images). For each Elementary Sampling Unit (ESU), the hemispherical images were processed using the CAN-EYE software (Version 4.2) developed at INRA-CSE. The derived biophysical variable maps are:

• four Leaf Area Index (LAI) are considered: effective LAI (LAIeff) and true LAI (LAItrue) derived from the measurement of the gap fraction as a function of the view zenith angle; effective LAI57 (LAI57eff) and true LAI57 (LAI57true) derived from the gap fraction at 57.5°, which is independent on leaf inclination. Effective LAI and effective LAI57 do not take into account clumping effect. LAItrue and LAI57true are derived using the method proposed by Lang and Xiang[1] (1986);

• cover fraction (fCover): it is the percentage of soil covered by vegetation. To improve the spatial sampling, fCover was computed over 0 to 10° zenith angle;

• fAPAR: it is the fraction of Absorbed Photosynthetically Active Radiation (PAR = 400-700nm). fAPAR is defined either instantaneously (for a given solar position) or integrated all over the day. Following a study based on radiative transfer model simulations, it has been shown that the root mean square error between instantaneous fAPAR computed every 30 minutes and the daily fAPAR is the lowest for instantaneous fAPAR at 10h00 AM (solar time, RMSE = 0.021). Therefore, the derivation of fAPAR from CAN-EYE corresponds to the instantaneous black sky fAPAR at 10h00 AM.

The land cover is mainly composed of vineyards with some areas of oaks. The detailed description of the site is available in the campaign report[2]. The site is quite flat (altitude: ≈ 100 m). It is approximately 3 x 3 km with coordinates described in Table 1:

| | UTM 31, North WGS-84 (units = meters) | | Geographic Lat/Lon WGS-84 (units = degrees) | |
|---|---|---|---|---|
| | Easting | Northing | Lat. | Lon. |
| Upper left corner | 654148.5000 | 4897307.0090 | 44.21269336 | 4.92956770 |
| Lower right corner | 657188.5000 | 4894267.0090 | 44.18469084 | 4.96668871 |
| Center | 655668.5000 | 4895787.0090 | 44.19869354 | 4.94813260 |

**Table 1. Description of the site coordinates.**

The ground measurements were carried out from 5th July to 9th July 2004, while the high spatial resolution image (SPOT2, HRV2, resolution: 20 m) was acquired on 29th June 2004.

# 2. Available data

## 2.1. SPOT Image

The SPOT image was acquired the 29th June 2004 by HRV2 on SPOT2. It was geo-located by SPOT image (SPOTView Basic product). The projection is UTM 31 North, WGS-84 (please, refer to the campaign report for more details: annex or http://www.avignon.inra.fr/valeri). No atmospheric correction was applied to the image since no atmospheric data were available. However, as the SPOT image is used to compute empirical relationships between reflectance and biophysical variable, we can assume that the effect of the atmosphere is the same over the whole 3 x 3 km site. Therefore, it will be taken into account everywhere in the same way.

Figure 1 shows the relationship between Red and near infrared (NIR) SPOT channels (no saturated points are observed).

[1] Lang, A.R.G. and Xiang, Y., 1986. Estimation of leaf area index from transmission of direct sunlight in discontinuous canopies. Agric. For. Meteorol., 37: 229-243.
[2] Annex or http://www.avignon.inra.fr/valeri

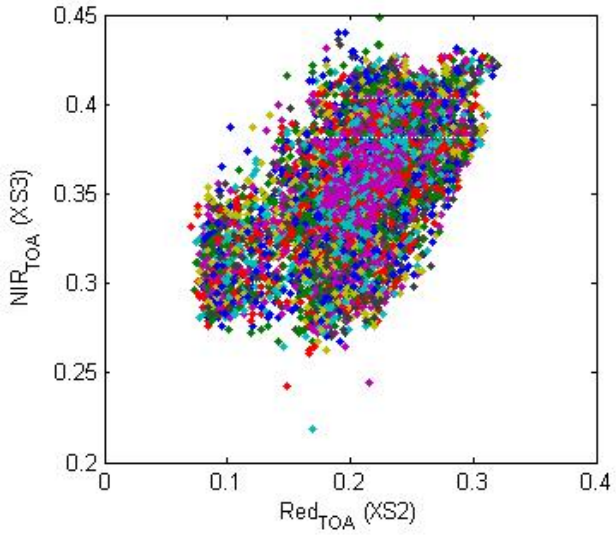


**Figure 1. Red/NIR relationship on the SPOT image for Plan-de-Dieu, 2004.**

## 2.2. Hemispherical images

The hemispherical images were processed using the CAN-EYE software (Version 4.2) to derive the biophysical variables. Figure 2 and Figure 3 show the distribution of the several variables over the 27 sampled ESUs. As Plan-de-Dieu site is mainly covered of vineyards, the hemispherical images were acquired from below the canopy. Note that there was understorey on E05 (oaks): hemispherical images were acquired from above the understorey and from below the canopy. The two sets of acquisition were processed separately to derived LAI (effective and true), LAI57 (effective and true), fCover, and fAPAR. The ESU biophysical variable was then computed as:

- LAIeff, LAI57eff, LAItrue, LAI57true: LAI(above) + LAI(below).
- fCover: 1-(1-fCover(above))*(1-fCover(below)). This assumes that independency of the gaps inside the understorey and the gaps inside the trees which is not true at all the scales but it is the only way to get the total fCover. However, for the local scales considered, this might be true as a first order approximation.
- fAPAR: [1-(1-fAPAR(below))*(1-fAPAR(above))], since 1-fAPAR can be considered equivalent to a gap fraction. Here again, the same independency between the two layers has to be assumed.

Note that LAI (effective and true) derived from directional gap fraction and LAI derived from gap fraction at 57.5° (effective and true) are consistent (Figure 2 and Figure 3). Effective LAI (LAIeff, LAI57eff) varies from 0.04 to 1.76, while true LAI (LAItrue, LAI57true) varies from 0.04 to 2.51. The site in terms of LAI is quite homogeneous since only one effective LAI value exceeds 0.83 (E05). LAIeff and LAI57eff are lower than LAItrue and LAI57true, due to the clumping observed for several ESUs. The relationship between fAPAR and LAI is in agreement with what is expected (Beer-Lambert law) while the fCover-LAI relationship is more noisy (Figure 3).

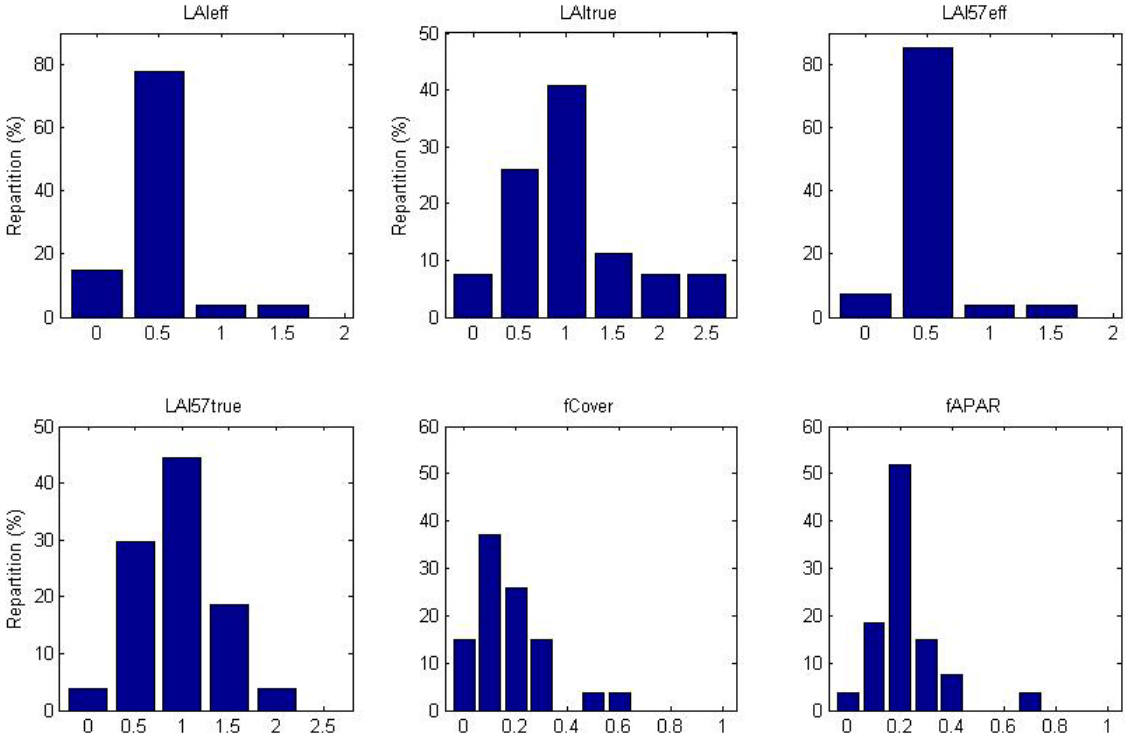


**Figure 2. Distribution of the measured biophysical variables over the ESUs.**

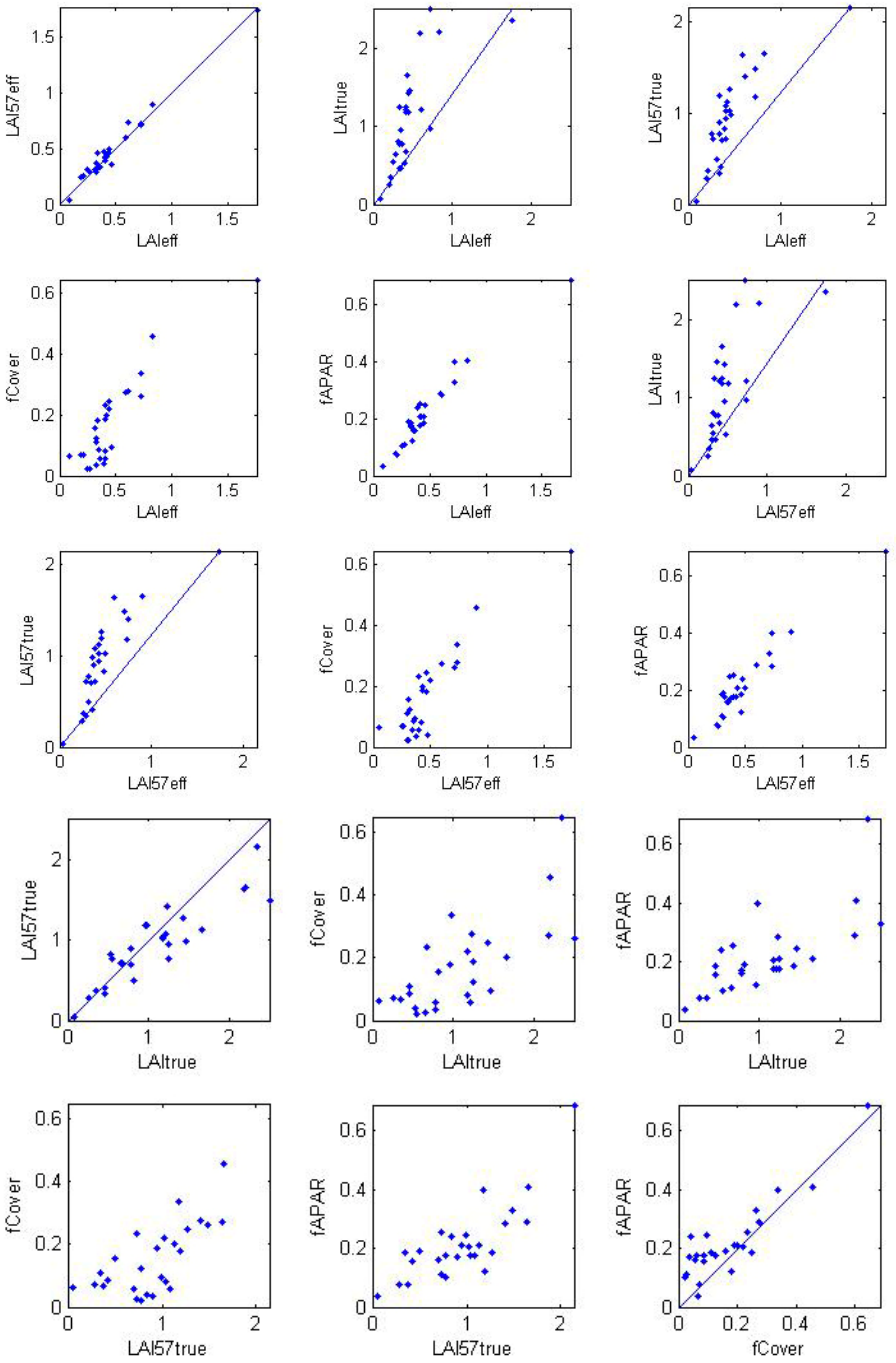


**Figure 3. Relationships between the different biophysical variables.**

## 2.3. Sampling strategy

### 2.3.1. Principles

The sampling strategy has been slightly modified as compared to other VALERI sites to be adapted to vineyards. It is defined in the campaign report[3].

Figure 4 shows that the 27 ESUs are evenly distributed over the site (3 x 3 km). The processing of the ground data has shown that: considering that SPOT geo-location and GPS measurements are associated to errors, E05 has been shifted by 1 SPOT pixel.

[3] Annex or http://www.avignon.inra.fr/valeri

Finally, all the ESUs have been kept for the computation of the transfer function.

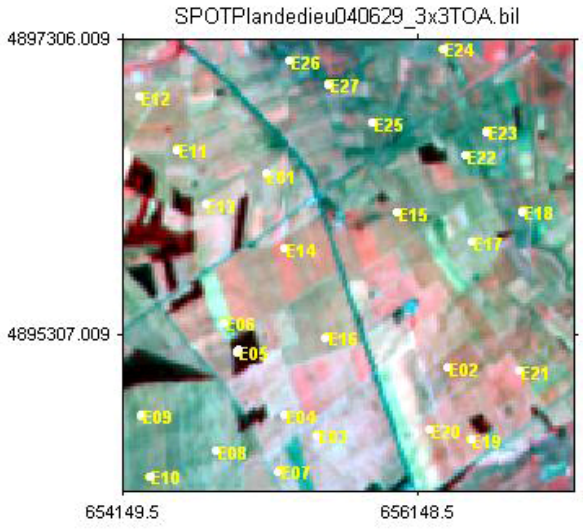


**Figure 4. Distribution of the ESUs around the Plan-de-Dieu site.**

### 2.3.2. Evaluation based on NDVI values

The sampling strategy is evaluated using the SPOT image by comparing the NDVI distribution over the site with the NDVI distribution over the ESUs (Figure 5). As the number of pixels is drastically different for the ESUs and whole site (WS = 22500 in case of a 3 x 3 km SPOT image), it is not statistically consistent to directly compare the two NDVI histograms. Therefore, the proposed technique consists in comparing the NDVI cumulative frequency of the two distributions by a Monte-Carlo procedure which aims at comparing the actual frequency to randomly shifted sampling patterns. It consists in:

1. computing the cumulative frequency of the *N* pixel NDVI that correspond to the exact ESU locations;
2. then, applying a unique random translation to the sampling design (modulo the size of the image);
3. computing the cumulative frequency of NDVI on the randomly shifted sampling design;
4. repeating steps 2 and 3, 199 times with 199 different random translation vectors.

This provides a total population of $N = 199 + 1$(actual) cumulative frequency on which a statistical test at acceptance probability $1 - \alpha = 95\%$ is applied: for a given NDVI level, if the actual ESU density function is between two limits defined by the $N\alpha/2 = 5$ highest and lowest values of the 200 cumulative frequencies, the hypothesis assuming that WS and ESU NDVI distributions are equivalent is accepted, otherwise it is rejected.

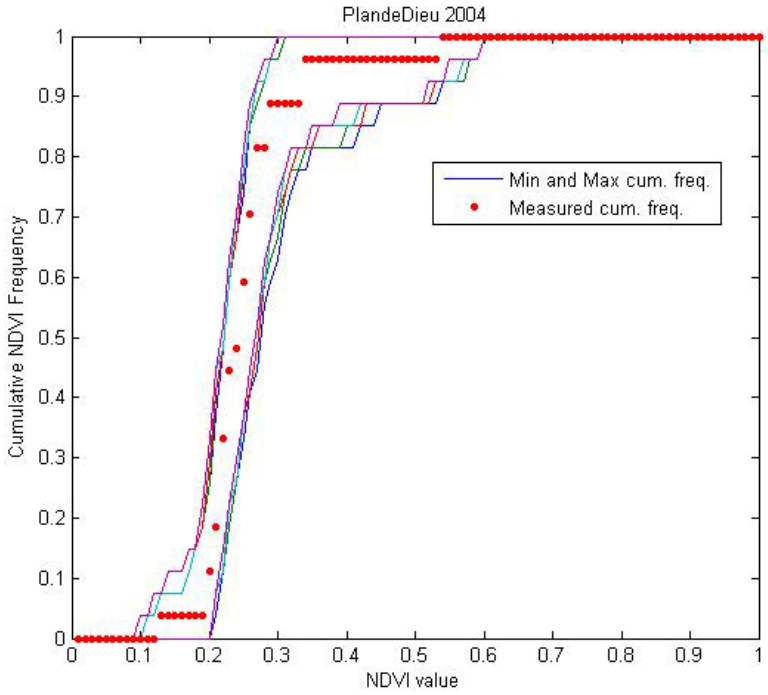


**Figure 5. Comparison of the ESU NDVI distribution and the NDVI distribution over the whole image.**

Figure 5 shows that the NDVI distribution of the 27 ESUs is very good over the whole site (comprised between the 5 highest and lowest cumulative frequencies). The site is homogeneous in terms of NDVI since the highest and lowest distributions are close.

### 2.3.3. Evaluation based on classification

A non supervised classification based on the k_means method (Matlab statistics toolbox) was applied to the 4 reflectances of the SPOT image to distinguish if different behaviours on the image for the biophysical variable-reflectance relationship exist.

A number of 5 classes was chosen (Figure 6). The distribution of the classes on the image and on the ESUs is comparable. Classes 1 and 5 are under-represented while classes 2, 3 and 4 appear to be over-sampled.

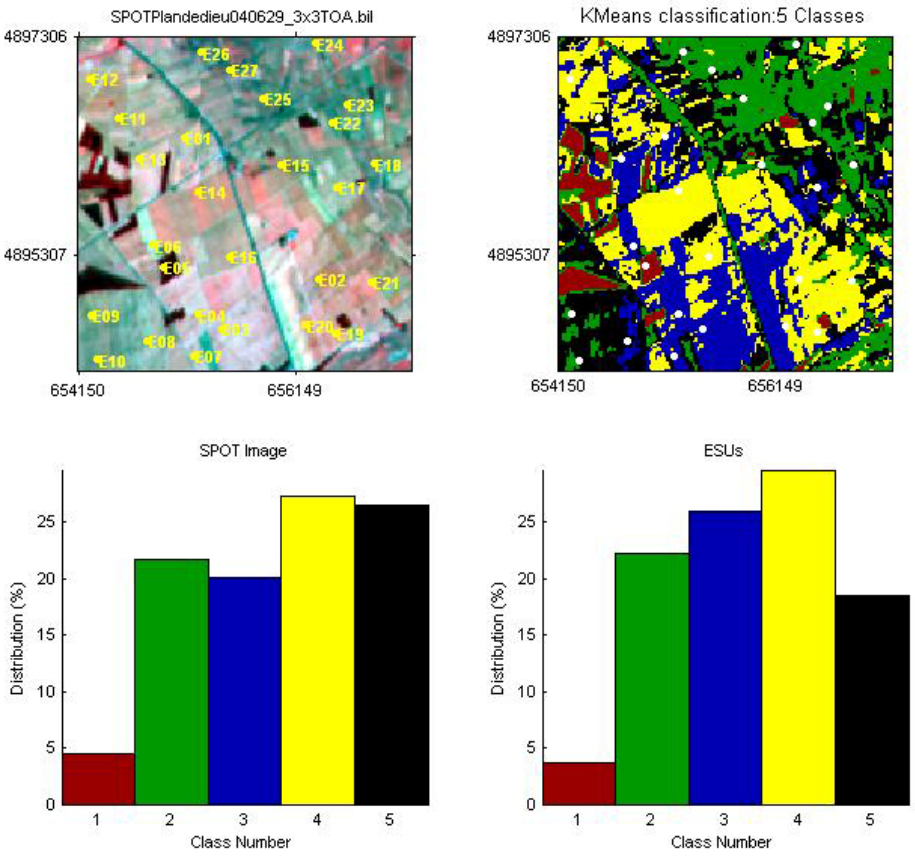


**Figure 6. Classification of the SPOT image. Comparison of the class distribution between the SPOT image and sampled ESUs.**

Figure 7 shows the different relationships observed between the biophysical variables and the corresponding NDVI on the ESUs, as a function of the SPOT classes determined from non supervised classification.

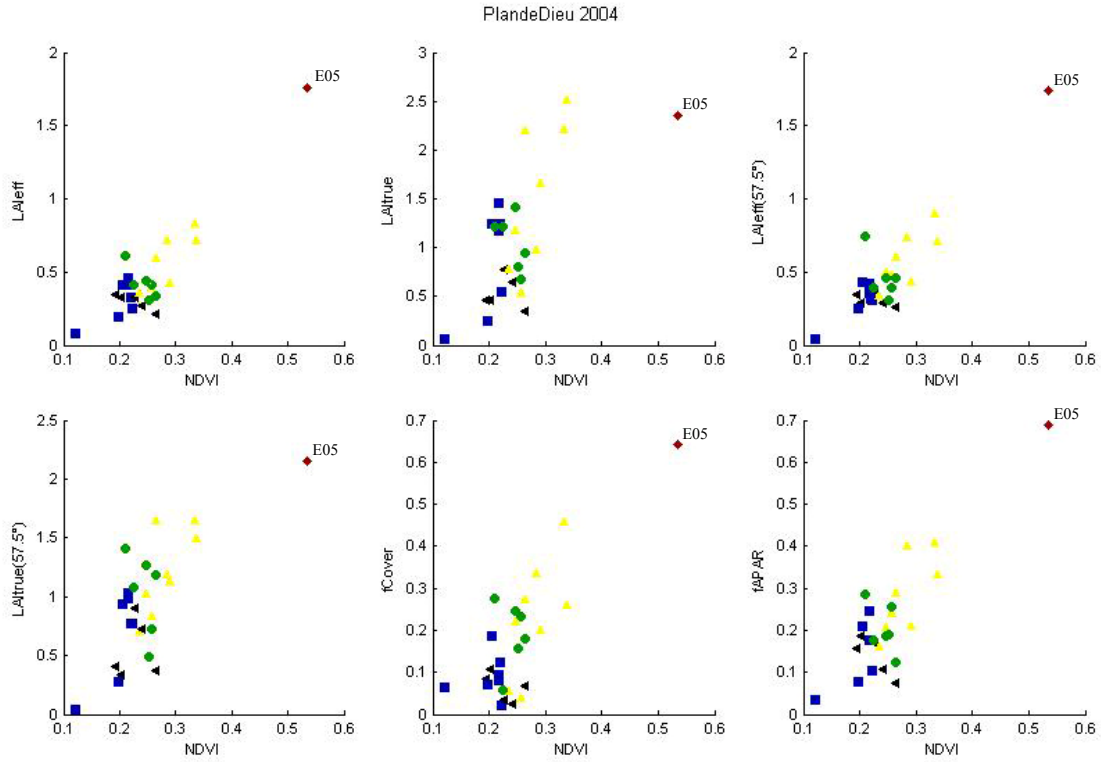


**Figure 7. NDVI-Biophysical Variable relationships as a function of SPOT classes**

The relation between NDVI and biophysical variables is consistent. The class 1 is represented by one ESU (E05). Note that there are not intermediate values between the class 1 (oaks) and the other classes (vineyards).

### 2.3.4. Using convex hulls

A test based on the convex hulls was also carried out to characterize the representativeness of ESUs. Whereas the evaluation based on NDVI values uses two bands (red and NIR), this test uses the four bands of the SPOT image. A flag image, is computing over the reflectances (Figure 8). The result on convex-hulls can be interpreted as:

- pixels inside the 'strict convex-hull': a convex-hull is computed using all the SPOT reflectance corresponding to the ESUs belonging to the class. These pixels are well represented by the ground sampling and therefore, when applying a transfer function the degree of confidence in the results will be quite high, since the transfer function will be used as an interpolator;
- pixels inside the 'large convex-hull': a convex-hull is computed using all the reflectance combination (±5% in relative value) corresponding to the ESUs. For these pixels, the degree of confidence in the obtained results will be quite good, since the transfer function is used as an extrapolator (but not far from interpolator);
- pixels outside the two convex-hulls: this means that for these pixels, the transfer function will behave as an extrapolator which makes the results less reliable. However, having a priori information on the site may help to evaluate the extrapolation capacities of the transfer function.

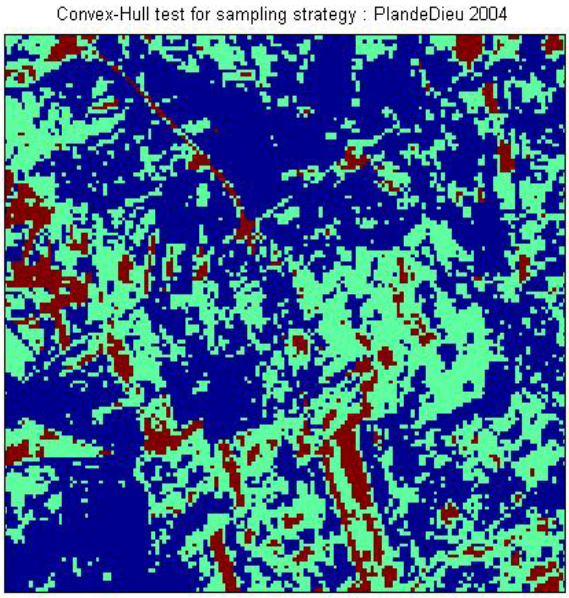


**Figure 8. Evaluation of the sampling based on the convex hulls. The map is shown: blue and light blue correspond to the pixels belonging to the 'strict' and 'large' convex hulls and red to the pixels for which the transfer function is extrapolating.**

This map shows that the representativeness of the ESUs is very good, even if a few pixels are outside the two convex-hulls. They correspond to roads, high NDVI pixels, bare soil…

# 3. Determination of the transfer function for the 6 biophysical variables: LAIeff, LAItrue, LAI57eff, LAI57true, fCover, fAPAR

## 3.1. The transfer functions considered

Two types of transfer functions are usually tested in the frame of the VALERI project:

- AVE: if the number of ESUs belonging to the class is too low. The transfer function consists only in attributing the average value of the biophysical variable measured on the class to each pixel of the SPOT image belonging to the class;

- REG: if the number of ESUs is sufficient, multiple robust regression between ESUs reflectance (or Simple Ratio) and the considered biophysical variable can be applied: we used the 'robustfit' function from the matlab statistics toolbox. It uses an iteratively re-weighted least squares algorithm, with the weights at each iteration computed by applying the bisquare function to the residuals from the previous iteration. This algorithm provides lower weight to ESUs that do not fit well. The results are less sensitive to outliers in the data as compared with ordinary least squares regression. At the end of the processing, three errors are computed: classical root mean square error (RMSE), weighted RMSE (using the weights attributed to each ESU) and cross-validation RMSE (leave-one-out method).

As the relationship between NDVI and LAI (§2.3.3) is consistent, the 'REG' method is applied to classes 2, 3, 4 and 5. If the 'REG' method is applied to all the ESUs (classes 1 to 5), the results are not pertinent since very high LAI values are estimated (LAI > 8). Therefore, the 'AVE' method is applied to the class 1. The biophysical variable values of E05 are thus attributed to 1019 pixels (4.4% of the site) of the SPOT image belonging to this class. Note that the average NDVI value of these pixels is equal to 0.49. The standard deviation and the variance are low (std = 0.066; var = 0.004). According with the people who acquired the data, E05 characterizes the areas of trees (oaks), even if the accuracy is not optimal.

The 'REG' function is tested using either the reflectance or the logarithm of the reflectance for any band combination as well as the simple ratio or NDVI. As the method has poor extrapolation capacities, a flag image, based on the convex hulls is computing over reflectances.

## 3.2. Results

### 3.2.1. Choice of the method

Except for E05 belonging to the class 1, a single transfer function was computed. Figure 9 shows the results obtained for all the possible band combinations using either the reflectance (ρ) or the logarithm of the reflectance (log(ρ)). Even if the regression made on the log(ρ) sometimes provides slightly better results, the results using the reflectance (ρ) were selected for all the variables. The transfer function using the log(ρ) indeed creates coplanar points which do not allow the determination of the 'strict' and 'large' convex hulls.

Note that the Red*NIR ('+' or RN) combination is added to all the band combinations (except for NDVI and SR). Please read the document: "a method to improve the relation between the biophysical variables" (http://www.avignon.inra.fr/valeri/table_methods/new_linear.pdf).

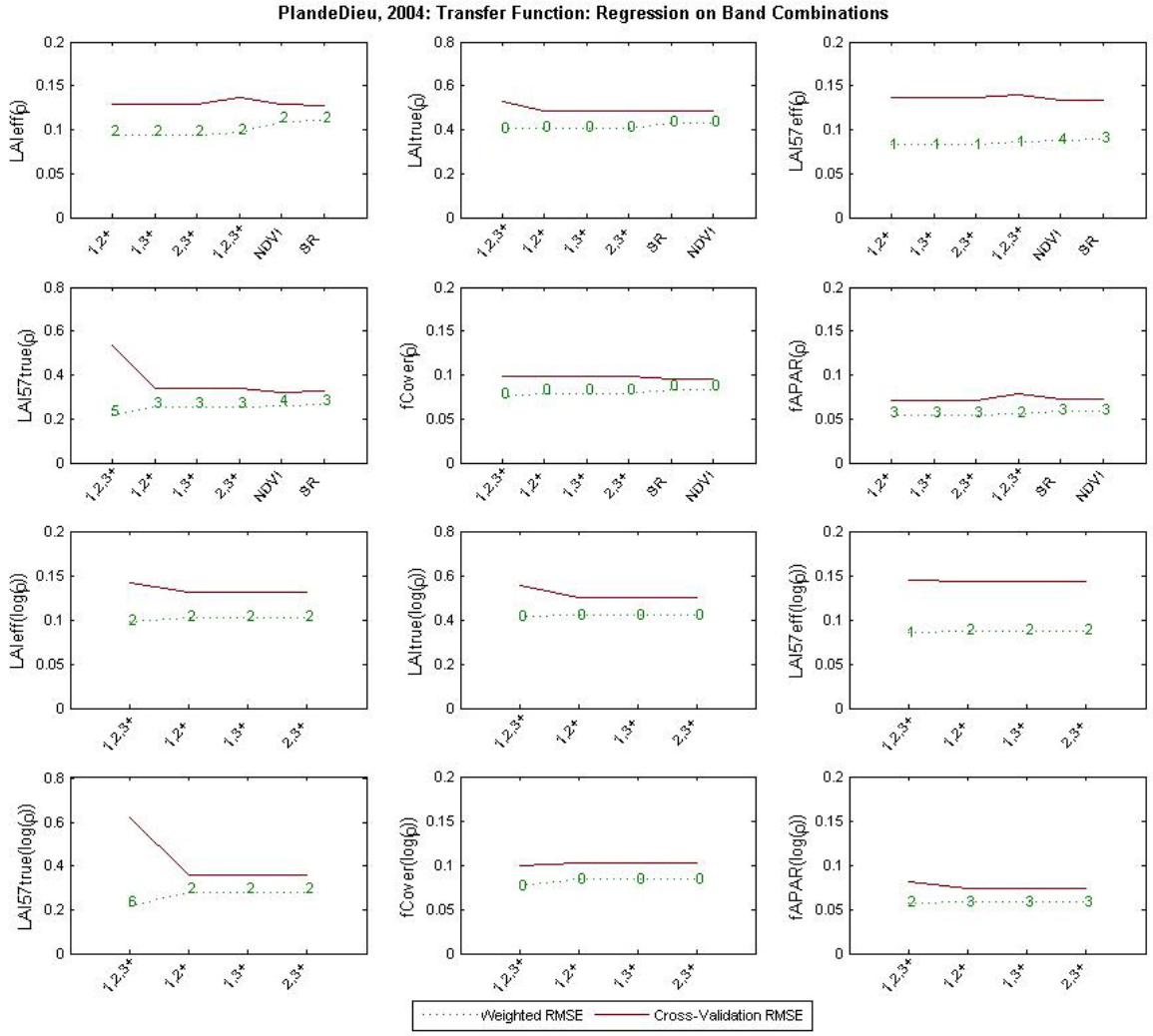


**Figure 9. Transfer function: test of multiple regression applied on different band combinations. Band combinations are given in abscissa. The estimated biophysical variable is given in ordinate. Top graphs correspond to regression made on reflectance (ρ): the weighted root mean square error (RMSE) is presented in green along with the cross-validation RMSE in red. The numbers indicate the number of data used for the robust regression with a weight lower than 0.7 that could be considered as outliers. Bottom graphs correspond to regression made on the logarithm of the reflectance.**

### 3.2.2. Choice of the band combination

**For the LAIeff**, the XS2, XS3, RN combination on reflectance (Figure 10 and Figure 11) was selected since it provides a good compromise between the cross-validation RMSE, the weighted RMSE (lowest value) and the

RMSE. Note that two weights are lower than 0.7. The following band combinations provide the same results: [XS1,XS2,RN] and [XS1,XS3,RN].

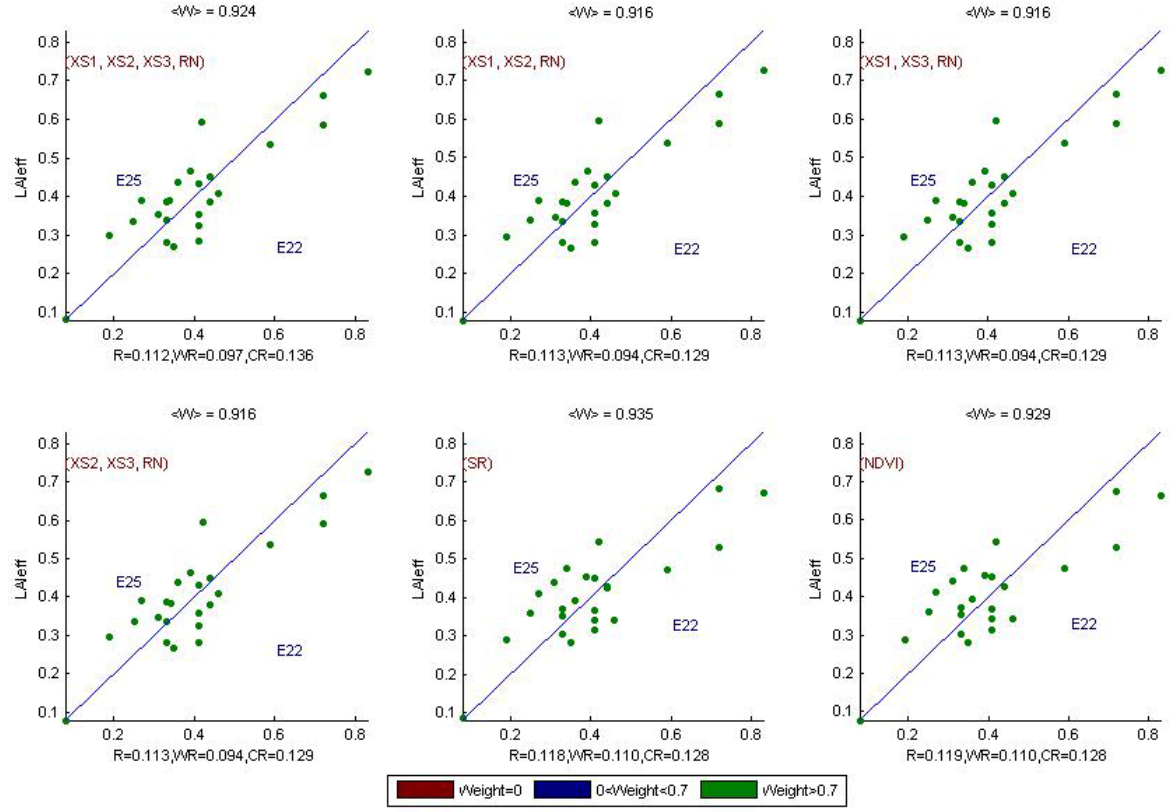


**Figure 10. Effective Leaf Area Index: results for regression on reflectance using different band combinations. R is the root mean square error computed between LAIeff and estimated LAIeff. WR is the weighted root mean square error and CR is the cross validation root mean square error.**

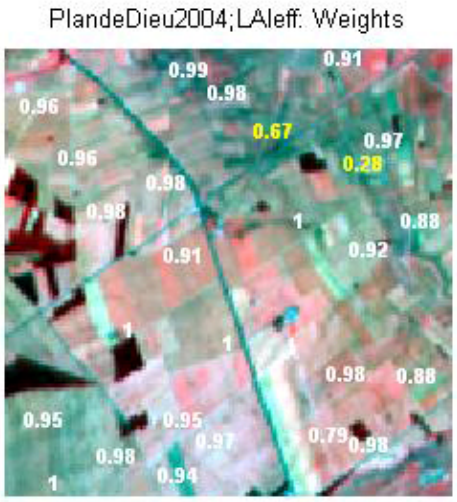


**Figure 11. Weights associated to each ESU for the determination of LAIeff transfer function.**

**For the LAItrue**, the XS2, XS3, RN combination on reflectance (Figure 12 and Figure 13) was selected since it provides a good compromise between the cross-validation RMSE (lowest value), the weighted RMSE and the RMSE. Note that no weight is lower than 0.7. The following band combinations provide the same results: [XS1,XS2,RN] and [XS1,XS3,RN].

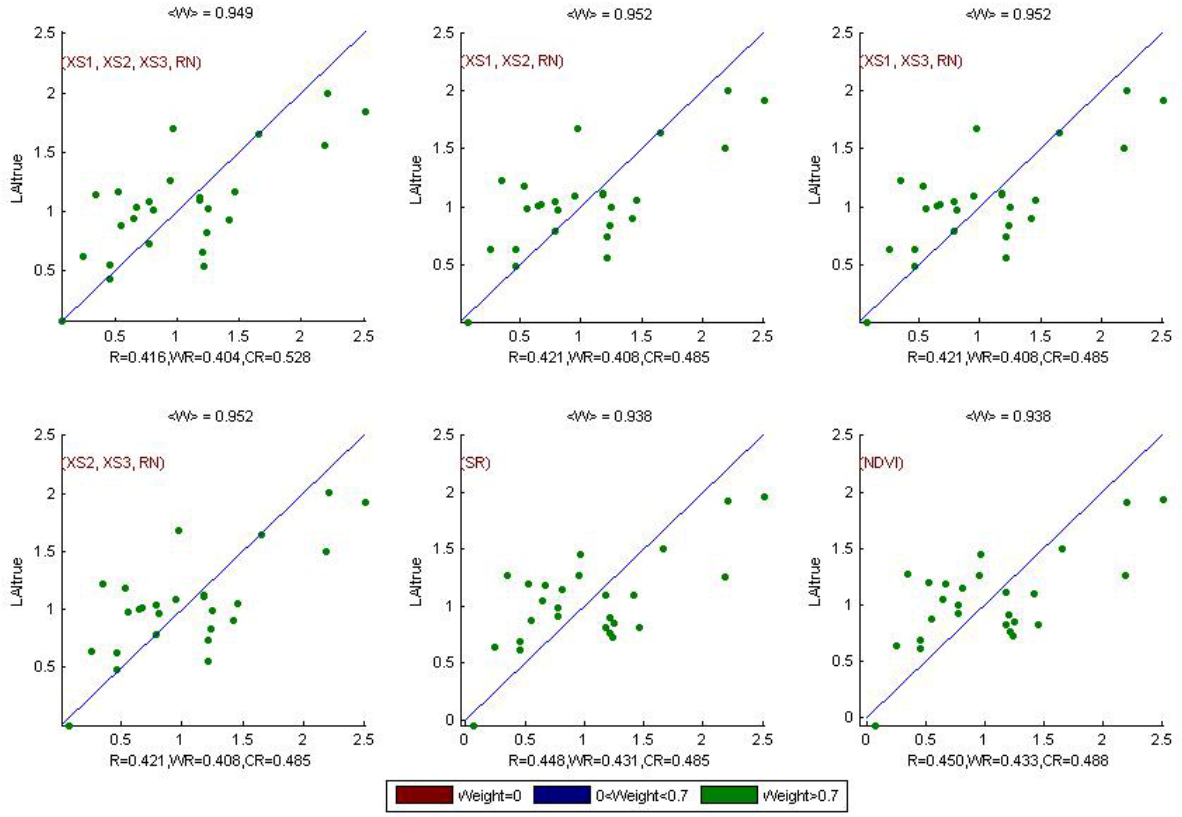


**Figure 12. True Leaf Area Index: results for regression on reflectance using different band combinations. R is the root mean square error computed between LAItrue and estimated LAItrue. WR is the weighted root mean square error and CR is the cross validation root mean square error.**

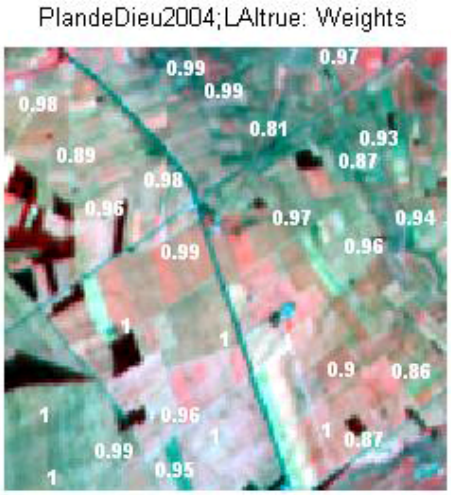


**Figure 13. Weights associated to each ESU for the determination of LAItrue transfer function.**

**For the LAI57eff**, the XS2, XS3, RN combination on reflectance (Figure 14 and Figure 15) was selected since it provides a good compromise between the cross-validation RMSE, the weighted RMSE (lowest value) and the RMSE. Note that one weight is lower than 0.7. The following band combinations provide the same results: [XS1,XS2,RN] and [XS1,XS3,RN].

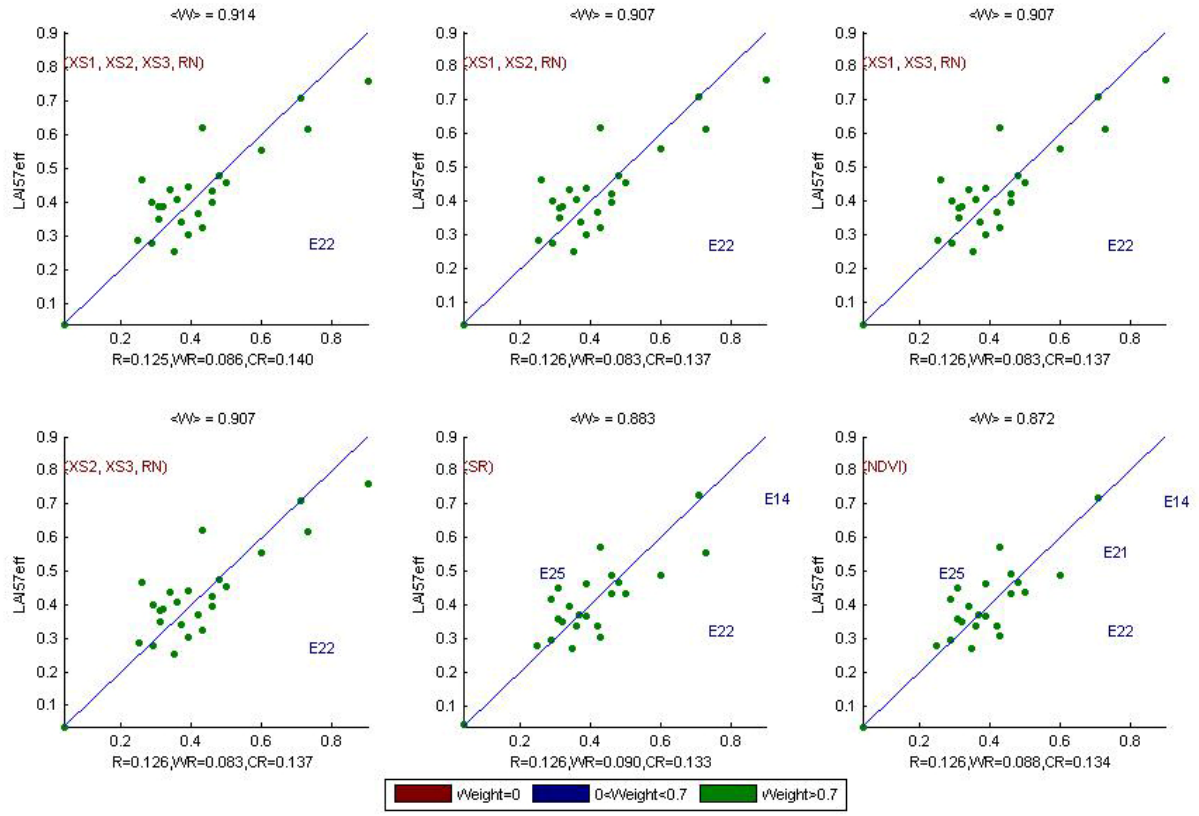


**Figure 14. Effective LAI at 57.5°: results for regression on reflectance using different band combinations. R is the root mean square error computed between LAI57eff and estimated LAI57eff. WR is the weighted root mean square error and CR is the cross validation root mean square error.**

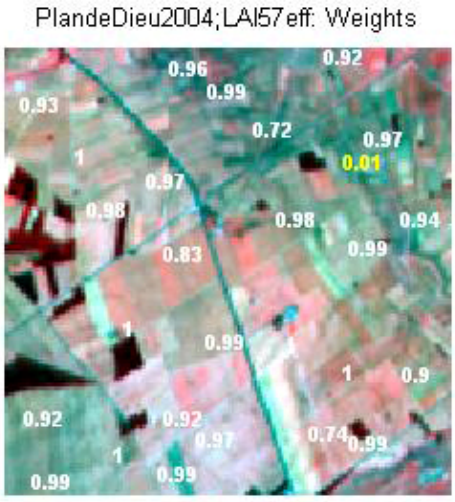


**Figure 15. Weights associated to each ESU for the determination of LAI57eff transfer function.**

**For the LAI57true,** the XS2, XS3, RN combination on reflectance (Figure 16 and Figure 17) was selected since it provides a good compromise between the cross-validation RMSE, the weighted RMSE (among the lowest values) and the RMSE (among the lowest values). Note that three weights are lower than 0.7. The following band combinations provide the same results: [XS1,XS2,RN] and [XS1,XS3,RN].

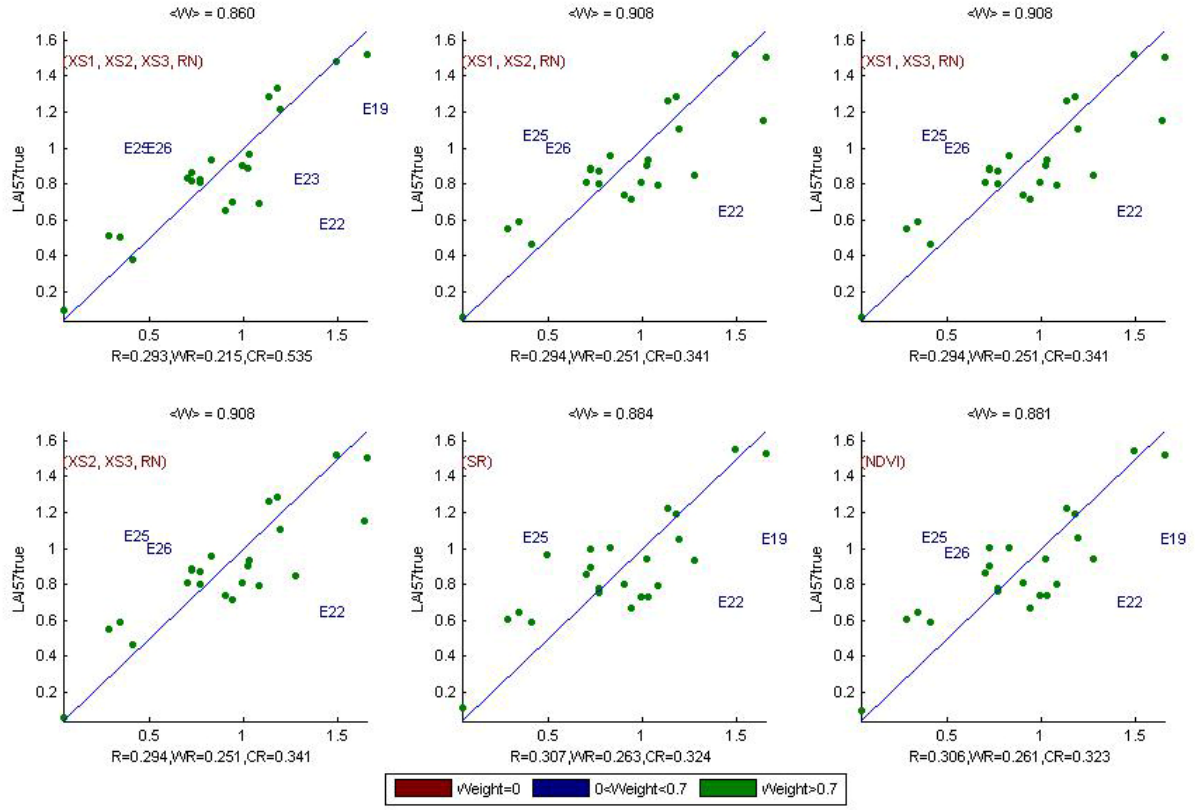


**Figure 16. True Leaf Area Index at 57.5°: results for regression on reflectance using different band combinations. R is the root mean square error computed between LAI57true and estimated LAI57true. WR is the weighted root mean square error and CR is the cross validation root mean square error.**

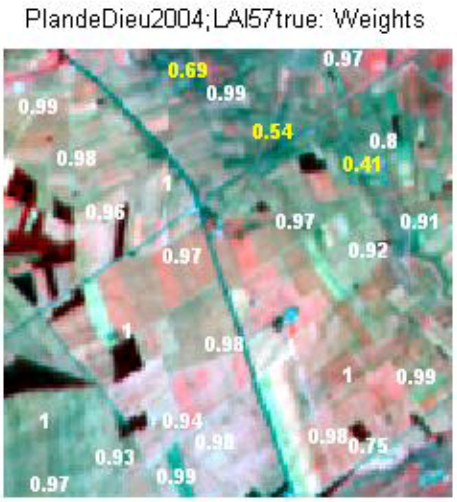


**Figure 17. Weights associated to each ESU for the determination of LAI57true transfer function.**

**For the fCover,** the XS1, XS2, XS3, RN combination on reflectance (Figure 18 and Figure 19) was selected since it provides the best results (except cross-validation RMSE). Note that no weight is lower than 0.7.

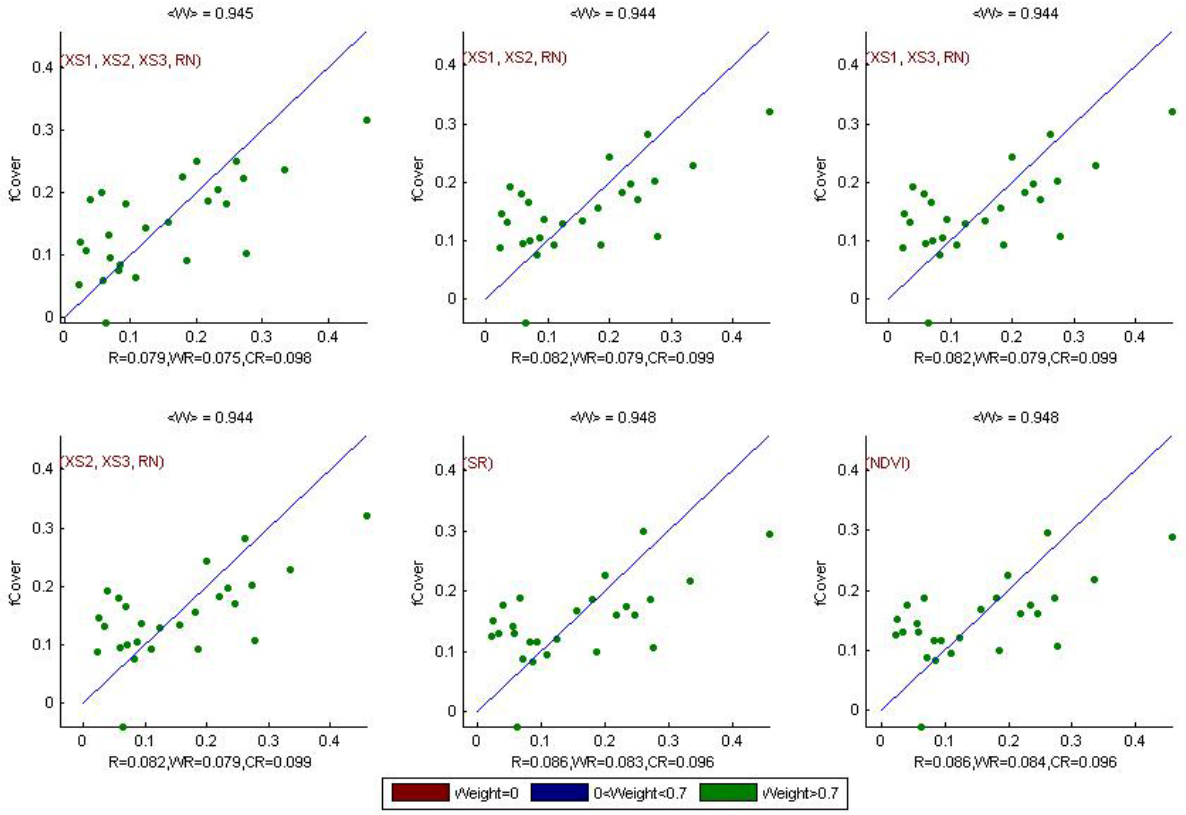


**Figure 18. fCover: results for regression on reflectance using different band combinations. R is the root mean square error computed between fCover and estimated fCover. WR is the weighted root mean square error and CR is the cross validation root mean square error.**

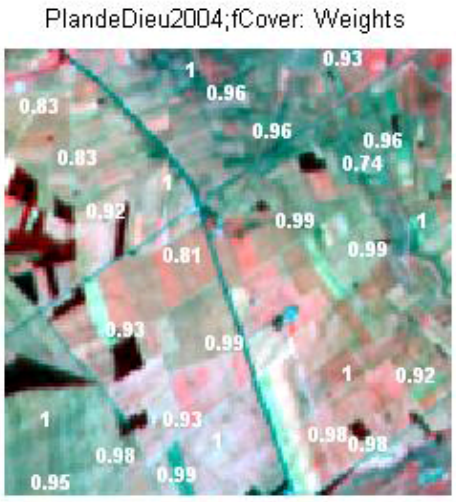


**Figure 19. Weights associated to each ESU for the determination of fCover transfer function.**

**For the fAPAR**, the XS2, XS3, RN combination on reflectance (Figure 20 and Figure 21) was selected since it provides the best results (except RMSE). Note that three weights are lower than 0.7. The following band combinations provide the same results: [XS1,XS2,RN] and [XS1,XS3,RN].

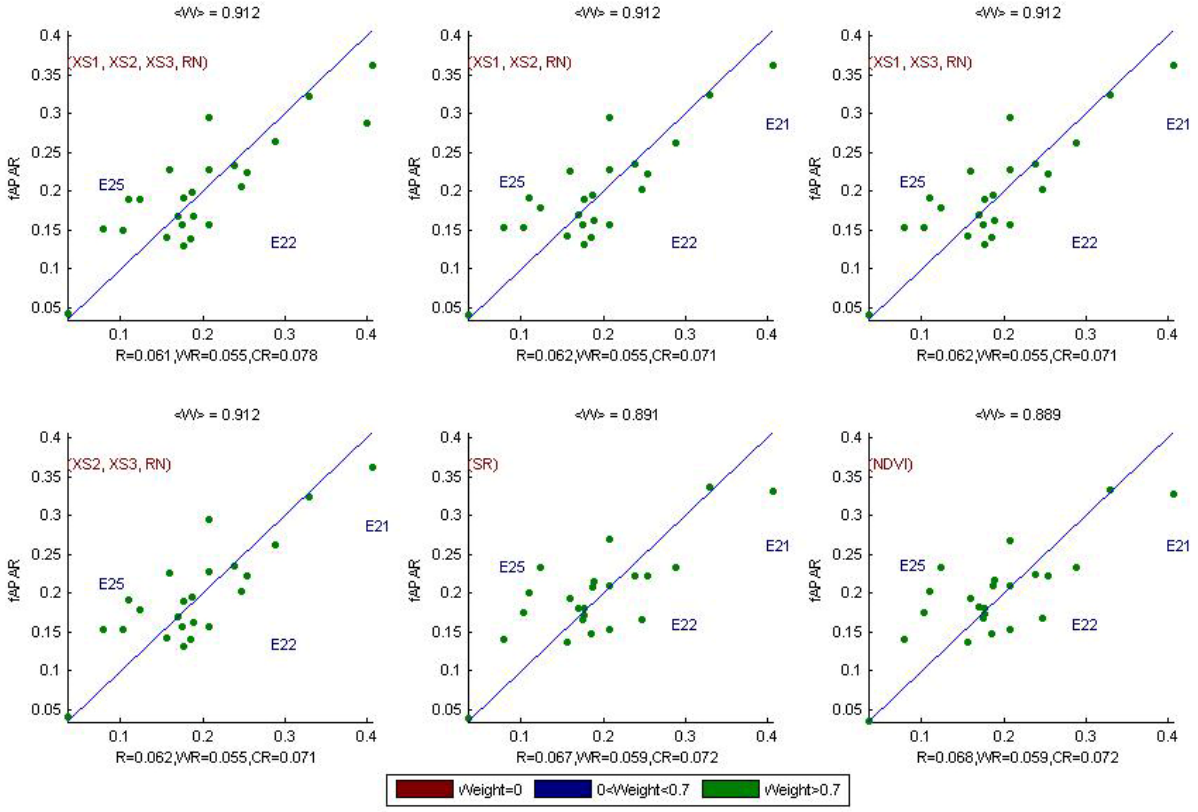


**Figure 20. fAPAR: results for regression on reflectance using different band combinations. R is the root mean square error computed between fAPAR and estimated fAPAR. WR is the weighted root mean square error and CR is the cross validation root mean square error.**

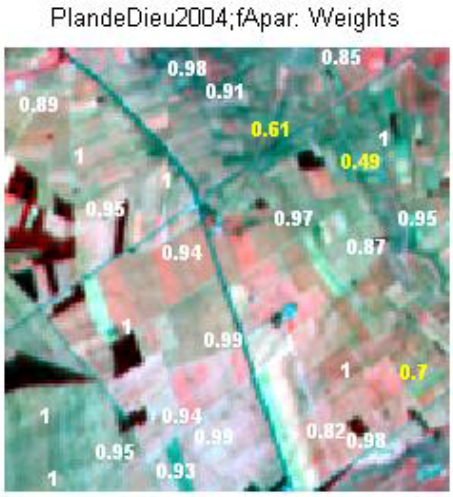


**Figure 21. Weights associated to each ESU for the determination of fAPAR transfer function.**

Following, the results of the transfer function (Table 2):

| Variable | Band Combination | RMSE | Weighted RMSE | Cross-valid RMSE |
|---|---|---|---|---|
| **LAIeff** | 1.9607 - 4.7448 (XS2) -12.078 (XS3) + 25.6746(RN) | 0.113 | 0.094 | 0.129 |
| **LAItrue** | 4.8094 + 4.7858(XS2) - 48.7644(XS3) + 75.6129(RN) | 0.421 | 0.408 | 0.485 |
| **LAI57eff** | 2.058 - 3.2655(XS2) - 14.2054(XS3) + 26.7887(RN) | 0.126 | 0.083 | 0.137 |
| **LAI57true** | 3.2612 + 11.0856(XS2) - 36.3633(XS3) + 43.2058(RN) | 0.294 | 0.251 | 0.341 |
| **fCover** | 4.4926 - 9.6743(XS1) - 17.4737(XS2) - 8.369(XS3) + 55.6965(RN) | 0.079 | 0.075 | 0.098 |
| **fAPAR** | 1.0747 - 4.1374(XS2) - 5.0093(XS3)+ 13.1796(RN) | 0.062 | 0.055 | 0.071 |

RN = Red*NIR

**Table 2. Transfer function applied to the whole site for the different biophysical variables, and corresponding errors**

## 3.3. Applying the transfer function to the Plan-de-Dieu SPOT image extraction

Figure 22 presents the biophysical variable maps obtained with the transfer function described in Table 2 for the classes 2, 3, 4 and 5 (class 1 corresponds to the trees; please read §3.1). The maps obtained for the six variables are consistent, showing similar patterns: low LAIeff values where low fCover or fAPAR are observed and conversely… The difference between effective LAI and true LAI is significant (see the average values in Figure 22). This was expected when looking the LAIeff/LAItrue relationship, showing that for high LAI the difference between the two can be significant.

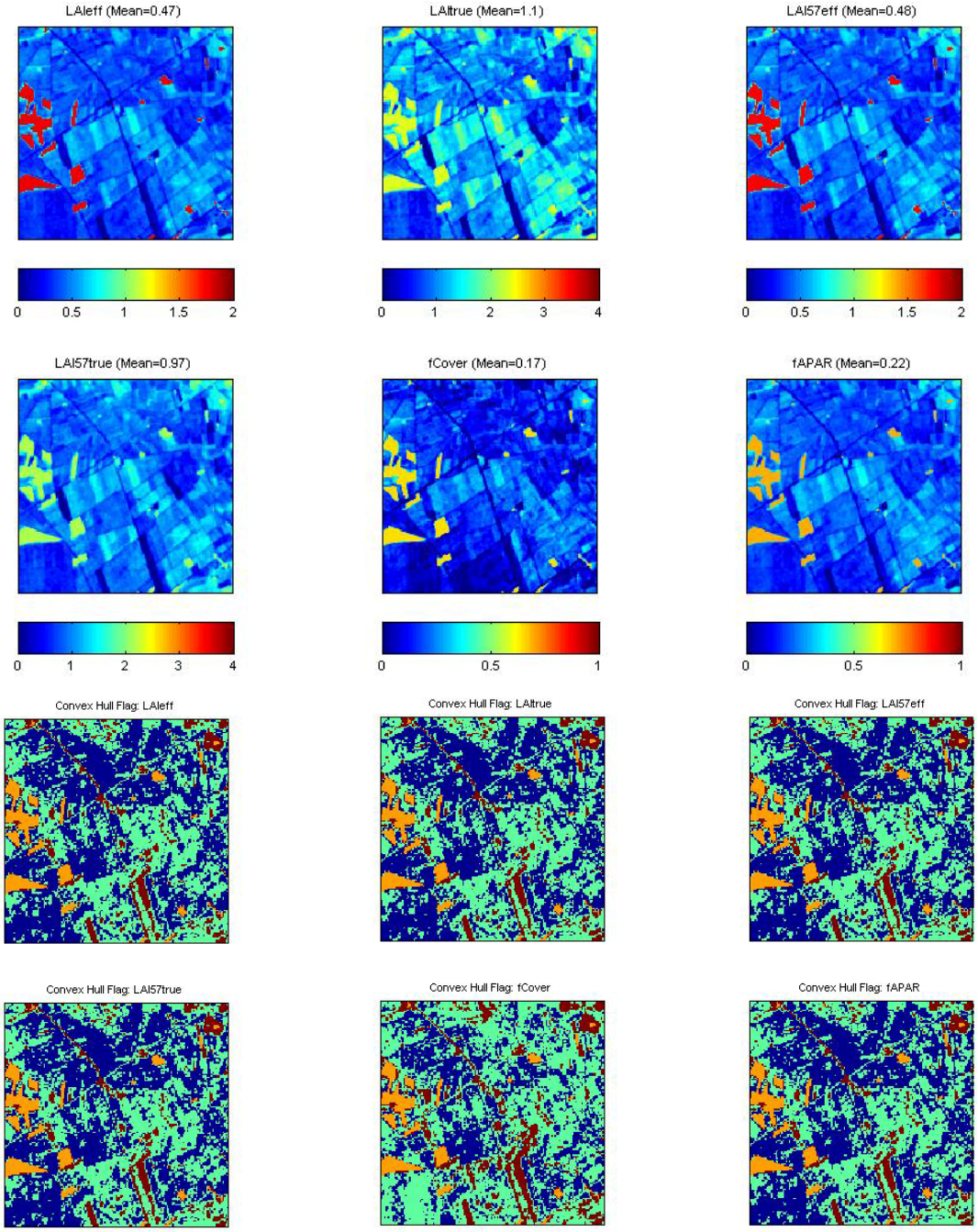


**Figure 22. High resolution biophysical variable maps applied on the Plan-de-Dieu site (top). Associated flags are shown: blue and light blue correspond to the pixels belonging to the 'strict' and 'large' convex hulls, red to the pixels for which the transfer function is extrapolating and orange to the pixels for which the 'AVE' transfer function is applied.**

The flag maps are comparable between LAIeff, LAItrue, LAI57eff, LAI57true and fAPAR (the number and the bands used for the regression are the same). The pixels outside the 'strict' convex hull are more numerous for fCover. This is due to the choice of the combinations. In theory, the more the number of bands increases, the larger the extrapolation is. The extrapolation mainly corresponds to roads, bare soil, high LAI pixels (§2.3.4)…

# 4. Conclusion

The 'REG' method is applied to the classes 2, 3, 4 and 5 by using 26 ESUs, whereas the 'AVE' method is applied to the class 1 which corresponds to areas of trees (oaks). The Plan-de-Dieu site is homogeneous in terms of LAI and NDVI. The relationship between these two variables is consistent. Note that the representativeness of

the land cover of the different ESUs is very good. The results of the robust regression are also good and the maps obtained for the biophysical variables are consistent. The flag associated to each map show that the little extrapolation of the transfer function is mainly bounded to roads, bare soil, high LAI pixels… For all the variables, the regression coefficients are computed by relating the variable itself to reflectance (§3.2.1).

The biophysical variable maps are available in UTM, 31 North, projection coordinates (Datum: WGS-84) at 20 m resolution.

## 5. Acknowledgements

We thank people who participated to the field experiment: **Nadine Bruguier**, **Kathy Pavageau**, **Olivier Marloie** (INRA CSE), **Marie Weiss** (Noveltis), but also **Iñaki Garcia de Cortazar Atauri** (INRA Agroclim), **Olivier Jacquet** (Chamber of Agriculture) and **the wine growers** which allowed us to visit their fields.

# ANNEX

# Ground measurement acquisition report for the VALERI site **Plan-de-Dieu**

sampled from 5th July 2004 to 9th July 2004

**M. Weiss[1], N. Bruguier[2]**
Organization: [1]NOVELTIS, [2]INRA CSE
email: marie.weiss@avignon.inra.fr

## Date of report 16 November 2004

People participating to the field experiment:

| Firstname & Name | 0rganization |
|---|---|
| N. Bruguier | INRA CSE |
| M. Weiss | NOVELTIS |
| K. Pavageau | INRA CSE |
| O. Marloie | INRA CSE |

# Site coordinates

| | Lat-Lon, WGS-84 (degrees) | | UTM 31 North, WGS-84 (meters) | |
|---|---|---|---|---|
| | Lat. | Long. | Easting | Northing |
| Upper left corner | 44.21262997 | 4.92958441 | 654150 | 4897300 |
| Lower right corner | 44.18499598 | 4.96621716 | 657150 | 4894300 |
| Center | 44.19881438 | 4.94790506 | 655650 | 4895800 |

# Ground control points

*This is extracted from the Excel file GPSplandeDieu2004.xls

| | | | | | | | | |
|---|---|---|---|---|---|---|---|---|
| GCP1 | A | 7 | 5 | 15 | 25 | 655466 | 4896261 | crossing Roads Rasteau/cairanne; Domaine Brusset |
| GCP2 | A | 7 | 5 | | | 655233 | 4896356 | path inside the vineyards, around ESU1 |
| GCP3 | A | 7 | 5 | 16 | 35 | 655200 | 4896341 | path inside the vineyards, around ESU1 |
| GCP4 | B | 7 | 6 | 10 | 21 | 656134 | 4894194 | crossing roads D23 / D8, "distillerie" |
| GCP5 | B | 7 | 6 | | | 656035 | 4894504 | first path on the left (W) "Bois des dames" |
| GCP6 | B | 7 | 6 | 10 | 34 | 655524 | 4894071 | end of the path, bare soil ploughed |
| GCP7 | B | 7 | 6 | 10 | 45 | 655104 | 4894493 | two pines crossing paths |
| GCP8 | B | 7 | 6 | 10 | 50 | 655331 | 4894667 | path, end of bare soil ploughed |
| GCP9 | B | 7 | 6 | 10 | 52 | 655388 | 4894711 | |
| GCP10 | B | 7 | 6 | 12 | 38 | 655092 | 4895177 | wood's East corner |
| GCP11 | B | 7 | 6 | 12 | 40 | 655016 | 4895375 | wood's North corner |
| GCP12 | B | 7 | 6 | 12 | 47 | 654853 | 4895267 | wood's West corner |
| GCP13 | B | 7 | 6 | 15 | 31 | 655259 | 4895113 | |
| GCP14 | B | 7 | 6 | 15 | 35 | 655855 | 4895075 | cedre crossing path |
| GCP15 | B | 7 | 6 | 16 | 18 | 654997 | 4894704 | little wood |

# Description of the site and land cover

## *Category according to IGBP classification*

Cropland.

## *Comments on the land cover*

The site corresponds to vineyards in the South East of France (“Côtes-du-Rhône Village”). Vineyards are very heterogeneous, aging from one year to several, and cultivated using different techniques (gobelet, palissage 1 fil, palissage 3 fils). Among the vineyards, some areas of trees (oaks) can be founded.

## *Topography*

The area is flat at about 100 m altitude.

## *Land cover map*

No land cover map is available.

# Spatial Sampling scheme

## *Sensors used for sampling the ESUs*

| | Method | Comments |
|---|---|---|
| ☒ | Hemispherical photographs | |
| ☐ | LAI2000 | |
| ☐ | TRAC | |
| ☐ | Ceptometer | |
| ☐ | Direct measurements | |
| ☐ | Other | |

## *Sampling strategy for the ESU*

The sampling strategy has been slightly modified as compared to other VALERI sites to be adapted to vineyards. The ESU is still 20mx20m, the sampling consists in acquiring 2x8 images along the ESU as described in figure 1:

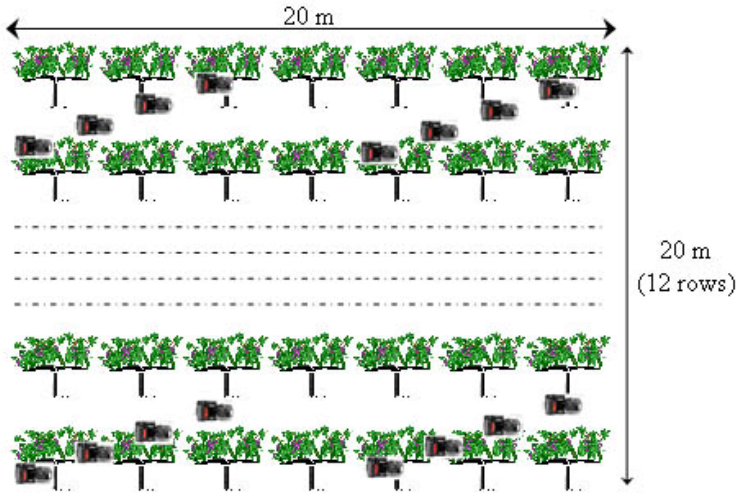


# The high spatial resolution image

## *Satellite*

| | |
|---|---|
| Satellite used | HRV2, SPOT 2 |
| Level of processing | SpotView Basic |
| Projection type | UTM 31 North, WGS-84 |
| Acquisition date | 29 June 2004 |

# List of the ESUs

| | | | | | | | | | |
|---|---|---|---|---|---|---|---|---|---|
| E01 | A | 7 | 5 | 16 | 17 | 655125 | 4896380 | 11.1 | vineyard |
| E02 | A | 7 | 5 | 16 | 50 | 656346 | 4895086 | 11.1 | vineyard |
| E03 | B | 7 | 6 | 11 | 53 | 655469 | 4894635 | 10.1,11.1 | vineyard, orientation: N/S |
| E04 | B | 7 | 6 | 12 | 24 | 655252 | 4894769 | 9,10.1,11.1 | vineyard |
| E05 | B | 7 | 6 | 14 | 25 | 654933 | 4895196 | 10.1,11.1 | wood |
| E06 | B | 7 | 6 | | | 654844 | 4895395 | 10.1,11.1 | young vineyard, height: 20 cm, row: N/S, no stone |
| E07 | B | 7 | 6 | 16 | 6 | 655217 | 4894391 | 9,10,11.1 | old vineyard |
| E08 | B | 7 | 6 | | | 654792 | 4894525 | 10.1,11.1 | vineyard |
| E09 | C | 7 | 7 | | | 654283 | 4894762 | 11.1 | vineyard, row: N/S |
| E10 | C | 7 | 7 | | | 654341 | 4894354 | 11.1 | vineyard, row: N/S |
| E11 | C | 7 | 7 | | | 654531 | 4896552 | 11.1 | od vineyard, row: N/S, height: 1.60 m |
| E12 | C | 7 | 7 | 15 | 35 | 654273 | 4896910 | 11.1,12.2 | vineyard, row: N/S, height: 1.20-1.50m |
| E13 | C | 7 | 7 | 15 | 55 | 654719 | 4896181 | 11.1 | vineyard, row: E/W, not very developed |
| E14 | C | 7 | 7 | 16 | 15 | 655250 | 4895882 | 11.1 | vineyard, irrigation |
| E15 | C | 7 | 7 | 16 | 35 | 656011 | 4896128 | 11,1 | vineyard, irrigation |
| E16 | B | 7 | 8 | 10 | 40 | 655536 | 4895292 | 8,11.1 | old vineyard, row: N/S |
| E17 | B | 7 | 8 | 11 | 18 | 656518 | 4895926 | 11.1 | sparse old vineyard, row: N/S |
| E18 | B | 7 | 8 | 11 | 40 | 656850 | 4896136 | 11.1 | vineyard, not much vegetation, row: N/S, no stone |
| E19 | B | 7 | 8 | 12 | 10 | 656505 | 4894598 | 11.1 | vineyard |
| E20 | B | 7 | 8 | 12 | 32 | 656233 | 4894671 | 11.1,12.2 | vineyard, row: N/S |
| E21 | B | 7 | 8 | 13 | 0 | 656832 | 4895061 | 11.1 | vineyard, row N/S |
| E22 | B | 7 | 8 | 14 | 45 | 656474 | 4896514 | 11.1 | vineyard, row: E/W |
| E23 | B | 7 | 8 | 15 | 2 | 656610 | 4896674 | 11.1,12.2 | vineyard |
| E24 | B | 7 | 8 | 15 | 25 | 656319 | 4897230 | 11.1 | vineyard, row: N/S |
| E25 | B | 7 | 8 | 15 | 52 | 655845 | 4896731 | 11.1 | old vineyard, row: N/S, no stone |
| E26 | B | 7 | 8 | 16 | 16 | 655283 | 4897147 | 11.1,12.2 | old vineyard, row: E/W, no stone |
| E27 | B | 7 | 8 | 16 | 40 | 655548 | 4896994 | | vineyard, row: N/S, dense vegetation |

# Acknowledgements

We want to thank Iñaki Garcia de Cortazar from INRA and Olivier Jacquet from the Agriculture chamber for their helpful comments on the site as well as the first visit. We also thank all the viticulturists who let us go on their fields for the measurements.